Politecnico di Torino

Porto Institutional Repository

[Article] Thin-walled beams subjected to load factors and non-structural masses

(Article begins on next page)

Thin-walled beams subjected to load factors and non-structural masses

E. Carrera [a,b], A. Pagani [a,*], F. Zangallo [a]

[a] *Department of Mechanical and Aerospace Engineering, Politecnico di Torino, Corso Duca degli Abruzzi 24, 10129 Torino, Italy* [b] *King Abdulaziz University, Jeddah, Saudi Arabia*

ABSTRACT

The static response of beam structures to inertial loads is investigated in this work. Refined beam models are adopted for the analyses due to the ineffectiveness of classical theories in dealing with three-dimensional (3D) phenomena. The Carrera Unified Formulation (CUF) has therefore been used to develop higher-order beam theories without the need of any ad hoc assumptions on the kinematics of the model. According to CUF, the 3D displacement field is expressed as the expansion, above the beam cross-section, of the generalized displacements, which lie along the beam axis. Different classes of refined one-dimensional (1D) models can be formulated, depending on the cross-sectional functions used for the expansion of the generalized unknowns. The weak form of the principle of virtual displacements is used in this paper and 1D finite element (FE) arrays are written in the form of fundamental nuclei, which do not depend on the class of the beam theory. Both closed and open thin-walled beams are considered in the proposed analysis, and the effects of uniform as well as arbitrarily distributed load factors are investigated. Non-structural masses are also contemplated. The results are compared with those obtained using solid finite elements from a commercial FE code. Attention is focussed on the need to adopt refined models because of the inability of classical beam theories to foresee cross-sectional deformations, shear effects, and bending-torsion couplings caused by non-symmetric inertial fields.

1. Introduction

In engineering practice, problems involving inertial loads and non-structural masses are of special interest. An important example is that of aerospace engineering. In aeronautical structure design, applied loads are, in fact, usually prescribed in terms of load factors, whereas non-structural masses are commonly used in finite element (FE) models to incorporate the weight of the engines and fuel. Moreover, non-structural mass distributions are occasionally employed to tune the inertial properties of the one-dimensional (1D) "stick" models of wings. Simplified 1D models are preferred in preliminary analyses in many fields of engineering due to their computationally efficiency and ease of use. However, it is well known that classical beam theories are not suitable for those problems that involve cross-sectional deformations, shear, and torsional effects, such as in the case of non-homogeneous distributions of acceleration fields. A brief overview of on classical and refined beam theories is given hereafter.

The classical and best-known beam theories are those by Euler [1] – hereafter referred to as EBBM – and Timoshenko [2,3] –

hereafter referred to as TBM. The former theory does not account for transverse shear deformations, whereas the latter assumes a uniform shear distribution along the cross-section of the beam, together with the effects of rotatory inertia. These models yield reasonably good results when slender, solid section, homogeneous structures are subjected to bending. However, the analysis of deep, thin-walled, open section beams may require more sophisticated theories to achieve sufficiently accurate results, see [4]. Over the last century, many refined beam theories have been proposed to over-come the limitation of classical beam modelling. Different approaches, including the introduction of shear correction factors, the use of warping functions based on de Saint-Venant's solution, the variational asymptotic method (VAM), the generalized beam theory (GBT), and others have been used to improve beam models. A general review of beam modelling, in which static, buckling, free-vibration and wave propagation analyses are taken into account, was proposed by Kapania and Raciti [5,6]. Some selective references and noteworthy contributions are discussed briefly below.

The early investigations focused on the use of appropriate shear correction factors to increase the accuracy of classical 1D formulations, see, for example, Timoshenko and Goodier [7], Sokolnikoff [8], Stephen [9], Hutchinson [10], and the recent work by Nguyen et al. [11]. However, a review paper by Kaneko [12] and a recent paper by Dong et al. [13], have highlighted the difficulty of defining a universally accepted formulation for shear correction

* Corresponding author. Tel.: +39 011 090 6870; fax: +39 011 090 6899.
E-mail addresses: erasmo.carrera@polito.it (E. Carrera), alfonso.pagani@polito.it (A. Pagani), francesco.zangallo@polito.it (F. Zangallo).

factors. Another important class of refinement methods reported in the literature is based on the use of warping functions. The contributions by El Fatmi [14,15], Ladevèze et al. [16], and Ladevèze and Simmonds [17] are some excellent examples. The asymptotic type expansion, in conjunction with variational meth-ods, was proposed in the work by Berdichevsky et al. [18], in which a noteworthy review of previous works on beam theory develop-ments is also given. Some recent valuable contributions on VAM are those by Rajagopal and Hodges [19], Wang and Yu [20], Yu and Hodges [21,22], and Kim and Wang [23]. The generalized beam theory was originally proposed by Schardt [24,25]. GBT improves classical theories through the use of a piece-wise beam description of thin-walled sections. GBT has been widely employed and extended in various forms by Silvetre [26], Nunes et al. [27], Silvestre and Camotim [28], and De Miranda et al. [29].

The response analysis of beam structures to load factors via higher-order theories is addressed in this paper. To the best of the authors' knowledge, a lack of papers on the static analyses of beams under arbitrary acceleration fields through refined models exists in the literature. This kind of analysis, in fact, requires the adoption of refined models, because of the inadequacy of EBBM and TBM theories to deal with non-classical effects. The Carrera Unified Formulation (CUF) is used in the present work to develop higher-order beam models, without the need of a priori kine-matics assumptions. CUF was initially devoted to refined plate and shell theories, see [30–32]. In recent works [33,34], CUF has been extended to beam modelling. Two classes of CUF 1D models have been proposed: the Taylor-expansion class, hereafter referred to as TE, and the Lagrange-expansion class, hereafter referred to as LE. TE models exploit N-order Taylor-like polynomials to define the displacement field above the cross-section with N as a free parameter of the formulation. The capacity of CUF TE models to deal with arbitrary geometries, thin-walled structures and to identify local effects is well known for both static [35,36] and free-vibration analyses [37–39]. The LE class is based on the use of Lagrange-like polynomials to discretize the cross-section displacement field. LE models have only pure displacement variables. Static analyses of isotropic [40] and composite structures [41] have revealed the capacity of LE models to deal with open cross-sections, arbitrary boundary conditions and to obtain *layer-wise* descriptions of the 1D model. LE models have recently been adopted successfully for the *component-wise* analysis of aeronautical structures [42,43] and civil engineering constructions [44,45].

Both TE and LE refined 1D models are used in this work and a finite element approximation is adopted along the beam reference axis to carry out the analysis of structures with arbitrary cross-section geometries and loading conditions. The FE approach can be used, in conjunction with CUF, to formulate stiffness matrices, load vectors derived from arbitrary acceleration fields, and non-structural masses in terms of fundamental nuclei, which do not depend upon either the order or the class of the beam theory that is implemented. Both open and closed homogeneous isotropic thin-walled structures subjected to inertial loads are analysed through the proposed methodology and the results are compared with those obtained using the MSC Nastran$^{©}$ commercial finite element method (FEM) code.

2. The 1D unified formulation

The notation assumed in this paper is hereinafter introduced. The adopted coordinate frame is presented in Fig. 1. Let **u** be the transposed displacement vector:

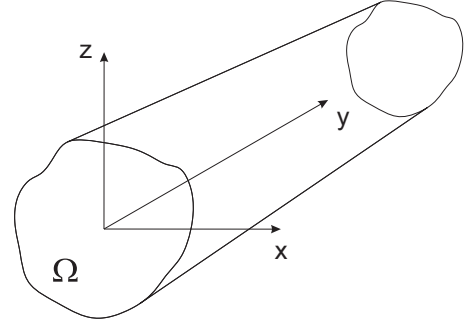$$\mathbf{u}(x,y,z) = \{u_x\ u_y\ u_z\}^T \tag{1}$$

Fig. 1. Coordinate frame of the beam model.

In the framework of the CUF, the displacement field above the cross-section is the expansion of generic functions, F_τ,

$$\mathbf{u}(x,y,z) = F_\tau(x,z)\mathbf{u}_\tau(y), \quad \tau = 1,2,\ldots,M \tag{2}$$

where F_τ vary over the cross-section. $\mathbf{u}_\tau$ is the displacement vector and M stands for the number of terms of the expansion. According to the generalized Einstein notation, the repeated subscript, τ, indicates summation. The choice of F_τ determines the class of the 1D CUF model that has to be adopted. TE (Taylor expansion) 1D models are based on polynomial expansions, $x^i z^j$, of the displacement field above the cross-section of the structure, where i and j are positive integers. For instance, the displacement field of the second-order ($N=2$) TE model is expressed by

$$u_x = u_{x_1} + xu_{x_2} + zu_{x_3} + x^2 u_{x_4} + xz u_{x_5} + z^2 u_{x_6}$$
$$u_y = u_{y_1} + xu_{y_2} + zu_{y_3} + x^2 u_{y_4} + xz u_{y_5} + z^2 u_{y_6}$$
$$u_z = u_{z_1} + xu_{z_2} + zu_{z_3} + x^2 u_{z_4} + xz u_{z_5} + z^2 u_{z_6} \tag{3}$$

The order N of the expansion, which can be set as an input of the analysis, is arbitrary and it defines the beam theory. Classical EBBM and TBM beam theories can be obtained as special cases of the linear ($N=1$) TE model as shown in [34].

The refined TE models described above are characterized by degrees of freedom (displacements and N-order derivatives of displacements) with a correspondence to the axis of the beam, see Fig. 2. The expansion can also be made by using only pure displacement values, e.g. by using Lagrange polynomials as cross-section functions F_τ. This class of CUF models, which is referred to as LE (Lagrange expansion), was recently introduced in [40], where triangular three- (L3) and six-node (L6) elements as well as quadrilateral four- (L4), nine- (L9) and 16-node (L16) elements were used to discretize the displacement unknowns on the cross-section of beam structures. In this paper, L9 polynomials are used. In the case of an L9 element the interpolation functions are given by

$$F_\tau = \frac{1}{4}(r^2 + rr_\tau)(s^2 + ss_\tau), \quad \tau = 1,3,5,7$$
$$F_\tau = \frac{1}{2}s_\tau^2(s^2 - ss_\tau)(1-r^2) + \frac{1}{2}r_\tau^2(r^2 - rr_\tau)(1-s^2), \quad \tau = 2,4,6,8$$
$$F_\tau = (1-r^2)(1-s^2), \quad \tau = 9 \tag{4}$$

where r and s vary from -1 to $+1$, whereas r_τ and s_τ are the coordinates of the nine points whose locations in the natural coordinate frame are shown in Fig. 3. The displacement field given by an L9 element is therefore

$$u_x = F_1 u_{x_1} + F_2 u_{x_2} + \cdots + F_9 u_{x_9}$$
$$u_y = F_1 u_{y_1} + F_2 u_{y_2} + \cdots + F_9 u_{y_9}$$
$$u_z = F_1 u_{z_1} + F_2 u_{z_2} + \cdots + F_9 u_{z_9} \tag{5}$$

where $u_{x_1}, \ldots, u_{z_9}$ are the displacement variables of the problem and represent the translational displacement components of each of the nine points of the L9 element. The beam model can be further refined by discretizing the beam cross-section with a
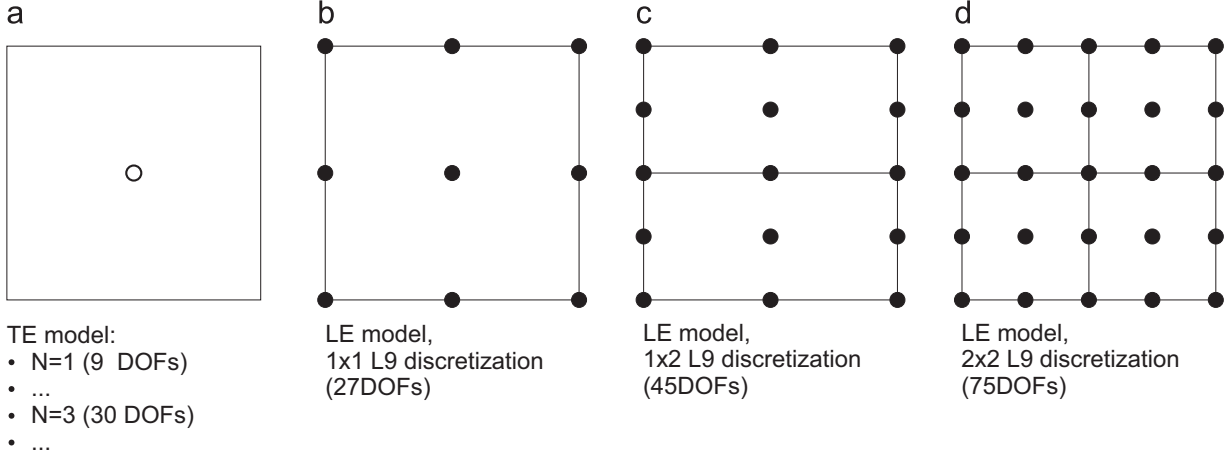
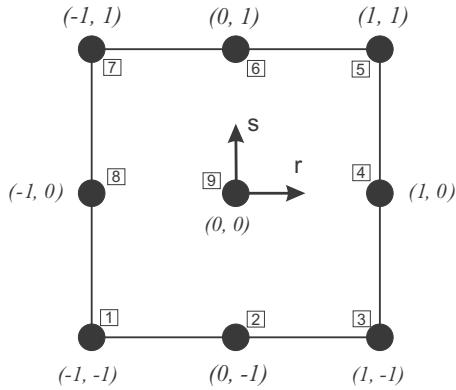Fig. 2. Differences between the TE and LE models.

Fig. 3. Cross-sectional L9 element.

number of L-elements as shown in [40]. For instance, different cross-sectional meshes in the case of a square section beam are shown in Fig. 2b–d.

2.1. Finite element formulation

The FE approach is adopted to discretize the structure along the y-axis. This process is conducted via a classical finite element technique, where the displacement vector is given by

$$\mathbf{u}(x,y,z) = F_\tau(x,z)N_i(y)\mathbf{q}_{\tau i} \tag{6}$$

N_i stands for the shape functions and $\mathbf{q}_{\tau i}$ for the nodal displacement vector,

$$\mathbf{q}_{\tau i} = \{q_{u_{x_{\tau i}}} \quad q_{u_{y_{\tau i}}} \quad q_{u_{z_{\tau i}}}\}^T \tag{7}$$

For the sake of brevity, the shape functions are not reported here. They can be found in many books, for instance in [46]. Elements with four nodes (B4) are adopted in this work, i.e. a cubic approximation along the y-axis is assumed. The choice of the cross-section discretization for the LE class (i.e. the choice of the type, the number and the distribution of cross-section elements) or the theory order, N, for the TE class is completely independent of the choice of the beam finite element to be used along the axis of the beam.

The stiffness matrix of the elements and the external loadings vector are obtained by means of the principle of virtual displacements

$$\delta L_{int} = \int_V (\delta \boldsymbol{\epsilon}^T \boldsymbol{\sigma}) \, dV = \delta L_{ext} \tag{8}$$

where L_{int} stands for the strain energy, L_{ext} is the work of the external loadings and δ stands for the virtual variation. ϵ and $\boldsymbol{\sigma}$ are

the strain and stress vectors, respectively. The virtual variation of the strain energy is rewritten using the constitutive laws, the linear strain-displacement relations and Eq. (6)

$$\delta L_{int} = \delta \mathbf{q}_{\tau i}^T \mathbf{K}^{ij\tau s} \mathbf{q}_{sj} \tag{9}$$

where $\mathbf{K}^{ij\tau s}$ is the stiffness matrix in the form of the fundamental nucleus. The derivation of the FE fundamental nucleus of the stiffness matrix is not repeated here for the sake of brevity, but it is given in [34], where more details about CUF can also be found. However, the components of the matrix $\mathbf{K}^{ij\tau s}$ are given in the following in the case of isotropic material:

$$K_{xx}^{ij\tau s} = (\lambda + 2G)\int_\Omega F_{\tau,x} F_{s,x} \, d\Omega \int_l N_i N_j \, dy + G\int_\Omega F_{\tau,z} F_{s,z} \, d\Omega \int_l N_i N_j \, dy$$
$$+ G\int_\Omega F_\tau F_s \, d\Omega \int_l N_{i,y} N_{j,y} \, dy$$

$$K_{xy}^{ij\tau s} = G\int_\Omega F_\tau F_{s,x} \, d\Omega \int_l N_{i,y} N_j \, dy$$

$$K_{xz}^{ij\tau s} = \lambda \int_\Omega F_{\tau,x} F_{s,z} \, d\Omega \int_l N_i N_j \, dy + G\int_\Omega F_{\tau,z} F_{s,x} \, d\Omega \int_l N_i N_j \, dy$$

$$K_{yx}^{ij\tau s} = G\int_\Omega F_{\tau,x} F_s \, d\Omega \int_l N_i N_{j,y} \, dy$$

$$K_{yy}^{ij\tau s} = G\int_\Omega F_{\tau,z} F_{s,z} \, d\Omega \int_l N_i N_j \, dy + G\int_\Omega F_{\tau,x} F_{s,x} \, d\Omega \int_l N_i N_j \, dy$$
$$+ (\lambda + 2G)\int_\Omega F_\tau F_s \, d\Omega \int_l N_{i,y} N_{j,y} \, dy$$

$$K_{yz}^{ij\tau s} = G\int_\Omega F_{\tau,z} F_s \, d\Omega \int_l N_i N_{j,y} \, dy$$

$$K_{zx}^{ij\tau s} = \lambda \int_\Omega F_{\tau,z} F_{s,x} \, d\Omega \int_l N_i N_j \, dy + G\int_\Omega F_{\tau,x} F_{s,z} \, d\Omega \int_l N_i N_j \, dy$$

$$K_{zy}^{ij\tau s} = G\int_\Omega F_\tau F_{s,z} \, d\Omega \int_l N_{i,y} N_j \, dy$$

$$K_{zz}^{ij\tau s} = (\lambda + 2G)\int_\Omega F_{\tau,z} F_{s,z} \, d\Omega \int_l N_i N_j \, dy + G\int_\Omega F_{\tau,x} F_{s,x} \, d\Omega \int_l N_i N_j \, dy$$
$$+ G\int_\Omega F_\tau F_s \, d\Omega \int_l N_{i,y} N_{j,y} \, dy \tag{10}$$

where G and λ are the Lamé's parameters. If Poisson's ratio ν and Young modulus E are used one has

$$G = \frac{E}{2(1+\nu)} \quad \text{and} \quad \lambda = \frac{\nu E}{(1+\nu)(1-2\nu)}$$

The fundamental nucleus has to be expanded according to the summation indexes τ and s in order to obtain the elemental stiffness matrix. It should be noted that $\mathbf{K}^{ij\tau s}$ does not depend

either on the expansion order or on the choice of the F_τ expansion polynomials. These are the key-points of CUF which allows, with only nine FORTRAN statements, the implementation of any-order of multiple class theories.

The loadings vector which is variationally coherent to the model can be derived with relative ease in the case of a generic concentrated load $\mathbf{P}$ acting on the application point (x_p, y_p, z_p):

$$\mathbf{P} = \{P_{u_x} \ P_{u_y} \ P_{u_z}\}^T \tag{11}$$

Any other loading condition can be similarly treated. The virtual work due to $\mathbf{P}$ is

$$\delta L_{ext} = \delta \mathbf{u}^T \mathbf{P} \tag{12}$$

After using Eq. (6), Eq. (12) becomes

$$\delta L_{ext} = F_\tau N_i \delta \mathbf{q}_{\tau i}^T \mathbf{P} \tag{13}$$

where F_τ and N_i are evaluated in (x_p, z_p) and y_p, respectively. The last equation allows the identification of the components of the nucleus which have to be loaded, that is, it allows the proper assembling of the loading vector by detecting the displacement variables that have to be loaded. In the next section, the attention is focussed on the special case of inertial loads.

2.2. Load factors and non-structural masses in the framework of CUF theories

When using classical beam theories, translational as well as rotational load factors are usually applied with respect to the reference axis – or with respect to the shear axis if transverse stresses are also included. In this paper, the capability of the present refined beam models to take into account the effects due to 3D distributions of inertial loads is investigated. Let the following acceleration field be applied to the structure:

$$\ddot{\mathbf{u}}_0(x, y, z) = \{\ddot{u}_{x_0} \ \ddot{u}_{y_0} \ \ddot{u}_{z_0}\}^T \tag{14}$$

The virtual variation of the external work, δL_{ext}, due to the acceleration field $\ddot{\mathbf{u}}_0$ is given by

$$\delta L_{ext} = \int_V \rho \delta \mathbf{u}^T \ddot{\mathbf{u}}_0 \, dV \tag{15}$$

where ρ is the density of the material. Eq. (6) is substituted into Eq. (15). It reads

$$\delta L_{ext} = \delta \mathbf{q}_{\tau i}^T \left[\int_\Omega \rho F_s F_\tau \left(\int_y N_i N_j \, dy \right) d\Omega \right] \ddot{\mathbf{q}}_{sj_0} \tag{16}$$

where the term between square brackets is the fundamental nucleus of the mass matrix $\mathbf{M}^{ij\tau s}$. The virtual variation of the external work is therefore written as

$$\delta L_{ext} = \delta \mathbf{q}_{\tau i}^T \mathbf{M}^{ij\tau s} \ddot{\mathbf{q}}_{sj_0} = \delta \mathbf{q}_{\tau i}^T \mathbf{P}_{ine}^{i\tau} \tag{17}$$

where $\mathbf{P}_{ine}^{i\tau}$ is the nucleus of the loading vector due to the acceleration field.

In the present work, rigid rotational accelerations $\ddot{\boldsymbol{\theta}}_0$ are also applied in order to provide comparisons with classical analyses. In this case, the loading vector is computed as above and by considering the acceleration field of Eq. (14) as

$\ddot{\mathbf{u}}_0 = \ddot{\boldsymbol{\theta}}_0 \times \mathbf{R}$ (18) where $\mathbf{R}$ is the distance vector between the center of the rotation and the loaded cross-sectional point in the case of LE models. In the case of TE models, the rigid rotational accelerations are directly applied to the degrees of freedom u_{z_2} and u_{x_3} (see Eq. (3)), which are responsible for the rigid rotation of the cross-section about the y-axis. However, it should be underlined that arbitrarily 3D distributed accelerations can be applied for both TE and LE.

In the present paper, the effect due to non-structural masses is also investigated. The non-structural masses can, in principle, be arbitrarily placed into the 3D domain of the beam structure. In the framework of the CUF, this is realized by adding the following term to the fundamental nucleus of the mass matrix:

$$\mathbf{m}^{ijts} = \mathbf{I}[F_\tau(x_m, z_m)F_s(x_m, z_m)N_i(y_m)N_j(y_m)]\tilde{m} \tag{19}$$

where $\mathbf{I}$ is the 3×3 identity matrix and $\tilde{m}$ is the non-structural mass applied at point (x_m, y_m, z_m).

3. Numerical results

The proposed beam formulation when dealing with load factors and non-structural masses is evaluated in this section and the results are compared with classical beam theories and solid FE models from the commercial code MSC Nastran©. Various homogeneous cross-section geometries made of an isotropic material are analyzed. The material adopted is an aluminium alloy and it has the following characteristics: Young modulus, E, equal to 75 GPa; Poisson ratio, ν, equal to 0.33 and density $\rho = 2700$ kg/m³. Unless differently specified, 10 B4 elements were used along the beam axis in the case of CUF models. The capability of the present 1D CUF theories to deal with refined solutions is demonstrated. Particular attention is focussed on the response to load factors of both closed and open thin-walled beams.

3.1. C-section beam

The analysis of a cantilever C-shaped beam was carried out as the first assessment. The cross-section of the structure is shown in Fig. 4 . The geometrical data are as follow s: $b = 0.5$ m, $a = h = 2b$ and $t = 0.1$ m. The length of the beam, , L is equal to 20 m. An inertial load was uniformly applied to the whole structure. The magnitude of the applied acceleration was equal to $1g$, with g the gravitational acceleration constant. The load was directed towards the negative direction of the z-axis.

Table 1 shows the maximum value of the vertical displacement, which is measured at $(0, L, h)$. Classical theories, EBBM and TBM, are given in the first rows for comparison purposes. Results by TE models from quadratic ($N=2$) to high-order polynomials ($N=9$) are considered. As far as the LE model is concerned, six L9 elements were used on the cross-section as shown in Fig. 5. Last rows of Table 1 contain the results by solid models from MSC Nastran©, which were obtained by using 8-node CHEXA elements. In particular, Solid A model was built with a mesh having the same nodes layout and the same number of degrees of freedom (DOFs) of the LE model. On the other hand, Solid B had a finer finite
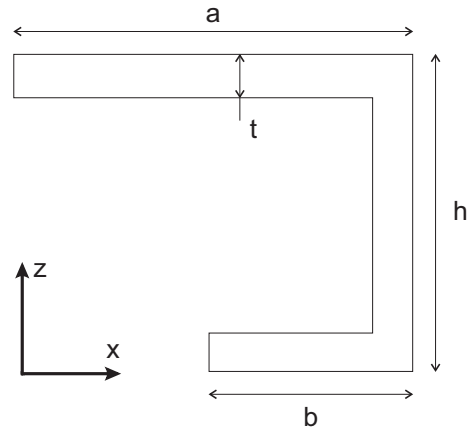

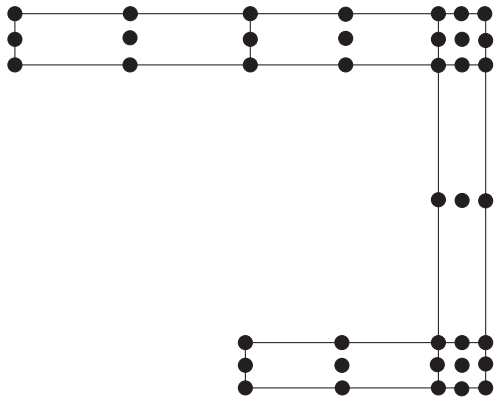**Fig. 4.** Cross-section of the C-shaped beam.

element mesh. In the third column of Table 1, the number of DOFs is also given for each model implemented. The following comments can be made:

- Classical beam theories are not effective in analysing the mechanical behaviour of the C-shaped thin-walled beam undergoing an uniform acceleration load; cross-section in-plane distortions are, in fact, neglected by EBBM and TBM.
- Increasingly accurate results are obtained as the theory-order (N) for TE models rises. However, Table 1 shows that higher-order TE models give errors ranging from 28% ($N=2$) to 5%($N=9$) with respect to the solid solution.
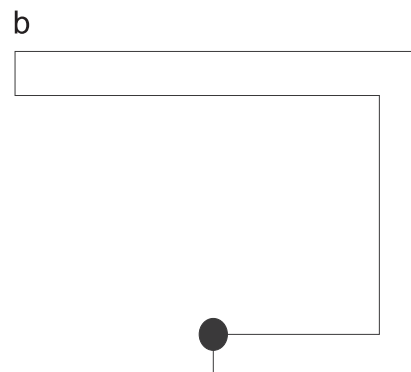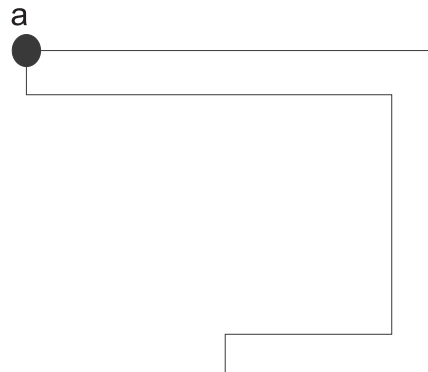
Table 1
Maximum value of the vertical displacement, u_z(m), at $(0, L, h)$, for the C-shaped beam under uniform inertial loading condition.

Models	$-u_z \times 10^2$	DOFs
Classical models		
EBBM	6.069	93
TBM	6.088	155
TE		
$N=2$	6.023	558
$N=4$	6.399	1395
$N=6$	7.242	2604
$N=7$	7.557	3348
$N=8$	7.796	4185
$N=9$	7.919	5115
LE		
6 L9, Fig. 5	8.277	3627
MSC Nastran		
Solid A	8.243	3627
Solid B	8.370	177,000

- The proposed LE model is able to detect the MSC Nastran© solid result.
- If displacements are compared, the proposed LE model seems to not improve solid models in terms of computational costs for the problem under consideration. In fact, displacement results by the 6 L9 model and Solid A are comparable.

Table 2
Vertical displacements, u_z (m), at the tip cross-section for the C-shaped beam undergoing acceleration loads and non-structural masses.

Models	Case A		Case B	DOFs
	$-u_z$ @ $(0, L, h)$	$-u_z$ @ (a, L, h)	$-u_z$ @ (a, L, h)	
Classical models				
EBBM	0.122	0.122	0.122	93
TBM	0.122	0.122	0.122	155
TE				
$N=2$	0.122	0.121	0.121	558
$N=3$	0.123	0.122	0.122	930
$N=4$	0.129	0.122	0.122	1395
$N=5$	0.135	0.123	0.123	1953
$N=6$	0.146	0.126	0.126	2604
LE				
6 L9, Fig. 5	0.167	0.127	0.127	3627
MSC Nastran				
Solid A	0.166	0.127	0.126	3627
Solid B	0.169	0.128	0.128	177,000

Undeformed	——
TE, N=5	– – – –
LE	–·–·–·
Nastran	×

Fig. 7. Tip cross-section deformation for the C-shaped beam (Case A). Comparison between CUF and Nastran Solid B models.

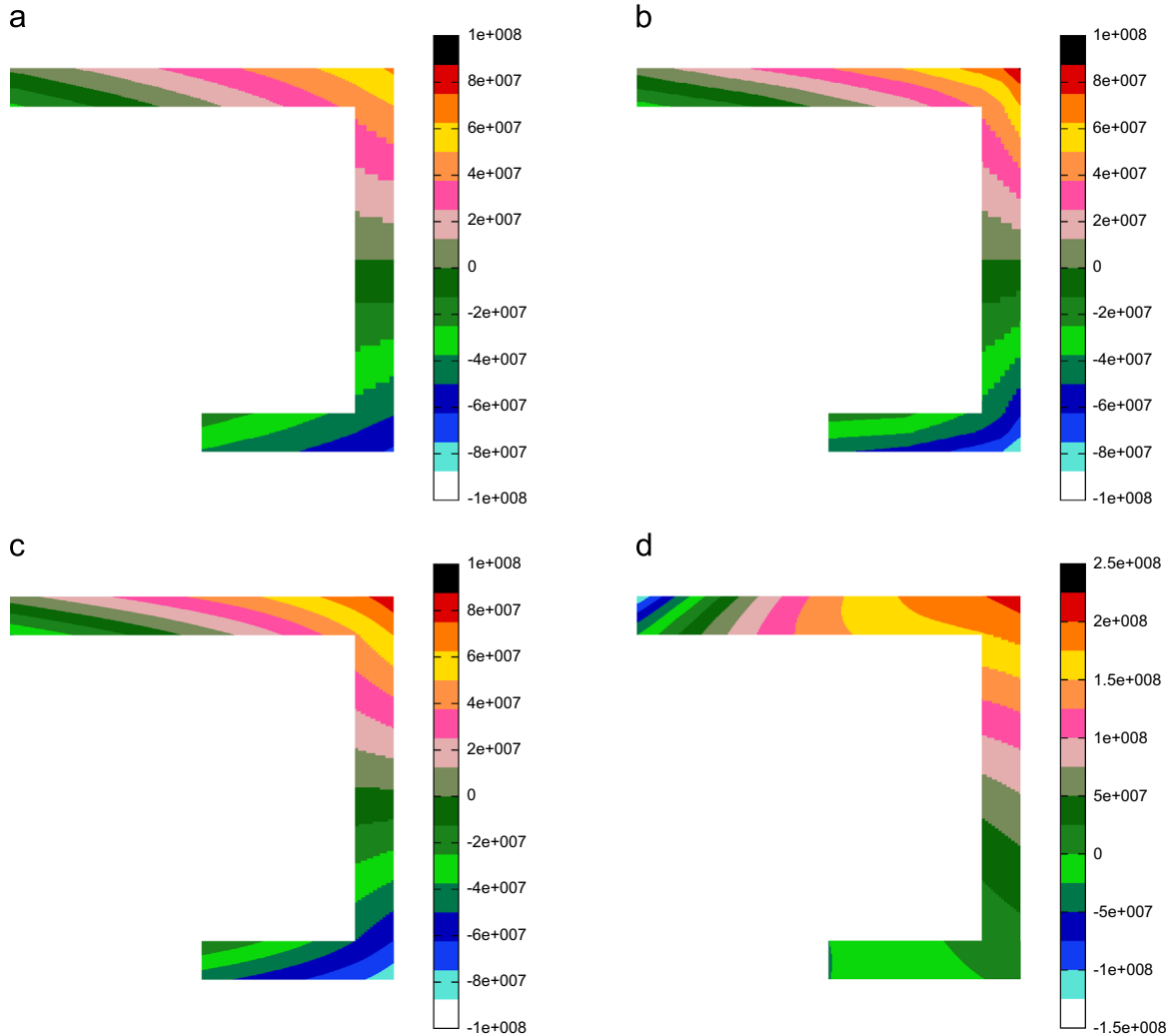**Fig. 5.** Distribution of L9 elements above the cross-section of the C-shaped beam.

a

b

Fig. 6. Position of the non-structural masses for the C-shaped beam: (a) Case A and (b) Case B.

Fig. 8. Distribution of axial stresses, σ_{yy}, at the clamped end ($y=0$) of the C-shaped beam (Case A): (a) Solid A model, (b) Solid B model, (c) LE 6 L9 model and (d) TE $N=5$ model.

In the second analysis case, a uniform load factor $n=2$ w a s applied in the negative direction of the z-axis and a non-structural mass equal to 40 kg was added at the coordinates $(0, L, h)$ as shown in Fig. 6a (Case A). The vertical component, u_z, of the displacements was measured at two different points on the tip cross-section and they are reported in the second and the third columns of Table 2. In Case B, the same uniform load factor $n=2$ as above was applied and the non-structural mass was placed as in Fig. 6b. For this configuration, the vertical displacement was measured at (a, L, h) and it is shown in the fourth column of Table 2. The number of the DOFs for each model implemented is also given in the last column of Table 2.

Fig. 7 shows the deformed configuration of the tip cross-section from fifth-order ($N=5$) TE, LE and MSC Nastran$^{©}$ Solid B models for Case A. For the same loading condition, cross-sectional distributions of axial, σ_{yy}, and transverse shear stresses, σ_{yz}, are shown in Figs. 8 and 9, respectively. Stress components for Case B are given in tabular form, see Table 3. It should be underlined that

- Unlike classical beam theories, higher-order TE and LE models are able to foresee cross-sectional deformations.
- Even tough high order of expansions are used, TE models are not able to deal with non-structural masses that are placed far

from the beam reference axis; both displacements and stress distributions are in fact not in good agreement with respect to the solid model.

- The results from the LE model match the MSC Nastran$^{©}$ Solid B solution both in terms of displacements and stress components.
- The computational efficiency of LE models is evident when stress eld components are accounted for. In fact, it is worth noting that Solid A model, which has the same DOFs of 6 L9 model, is completely inefficient for the computation of stresses.

3.2. I-shaped beam

A cantilevered I-shaped beam was subsequently considered. The cross-section geometry is shown in Fig. 10. The length of the structure, L, is equal to 3 m. The dimensions a and b are 0.2 m and 0.3 m, respectively. The thicknesses of both the flanges and the web are $t=0.05$ m.

The structure was subjected to a unitary uniform load factor ($1g$) directed along the negative direction of the z-axis in the first analysis case, and the results are shown in Table 4. Both displacement and stress components are given along with the number of DOFs for each models implemented. In particular, the vertical
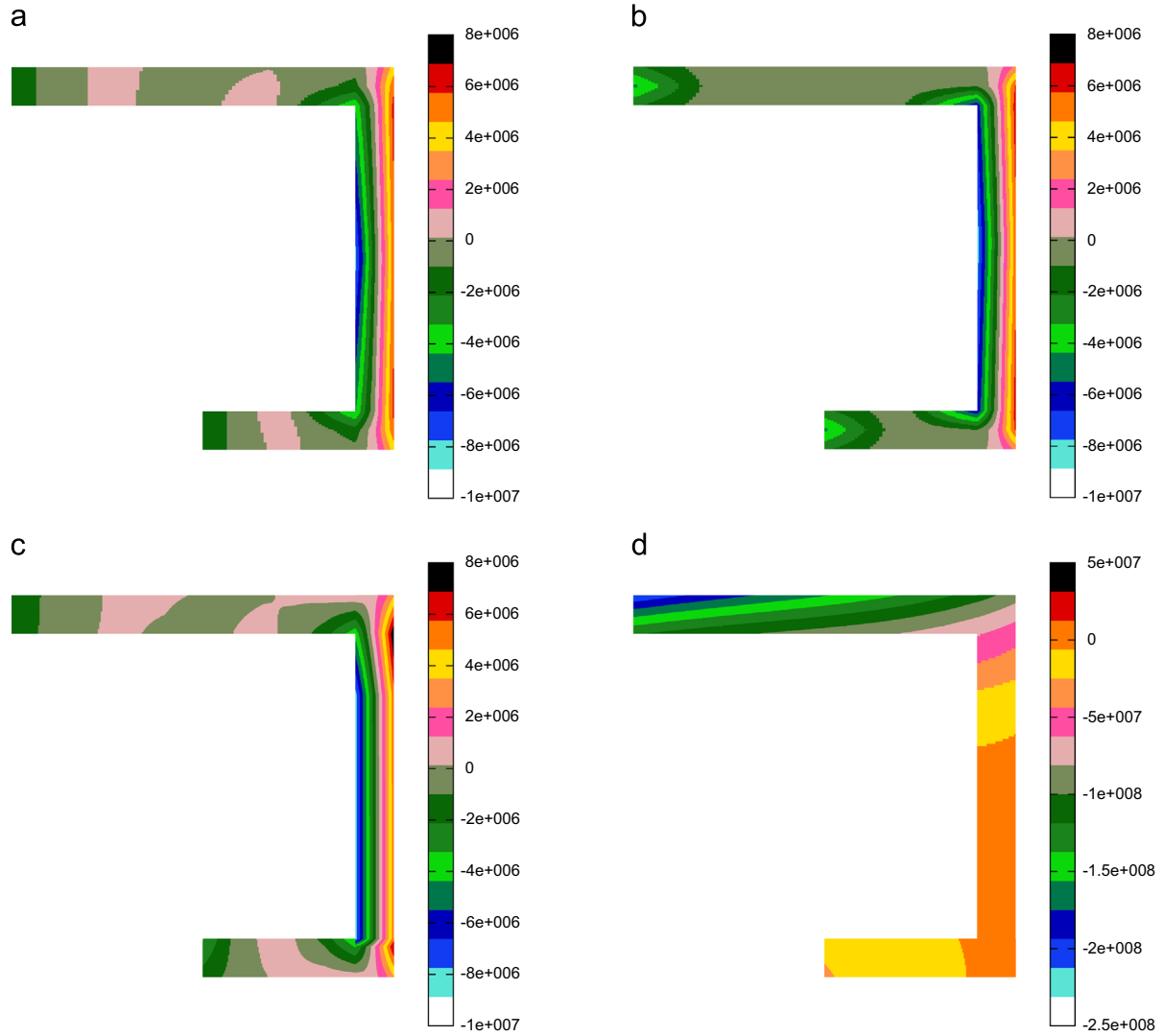
Fig. 9. Distribution of transverse shear stresses, σ_{yz}, at the mid-span ($y=L/2$) cross-section of the C-shaped beam (Case A): (a) Solid A model, (b) Solid B model, (c) LE 6 L9 model, and (d) TE $N=5$ model.
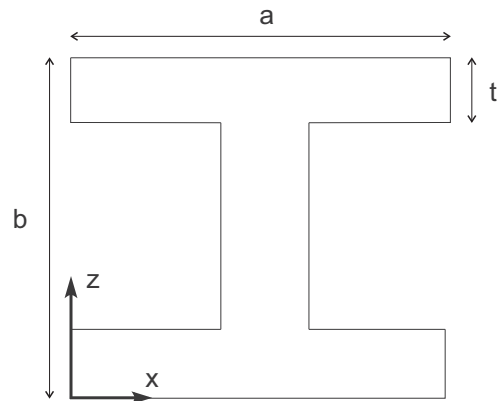
Table 3
Stress components σ_{yy} (MPa) at $(a, 0, h)$ and σ_{yz} (MPa) at $(a-t/2, L/2, h/2)$. C-shaped beam (Case B).

Models	$\sigma_{yy} \times 10^{-1}$	σ_{yz}	DOFs
	Classical models		
EBBM	9.748	0.000	93
TBM	9.748	-0.521	155
	LE		
6 L9, Fig. 5	8.451	-2.703	3627
	MSC Nastran		
Solid A	6.427	-1.344	3627
Solid B	8.906	-3.012	177,000

Fig. 10. Cross-section of the I-shaped beam.

displacement u_z at (a, L, b), the normal stress σ_{yy} at $(a/2, 0, b)$, and the shear stress σ_{yz} at $(a/2, L/2, 0)$ are reported. Both classical and refined TE models are considered in the first rows of Table 4. The results by the LE model are shown in row 11. The LE model was discretized by means of 7 L9 elements on the cross-section as shown in Fig. 11. A MSC Nastran[©] solid model was also built by means of 8-node CHEXA brick elements and the results are given in the last row for comparison purposes.

In the second analysis case, a non-structural mass equal to 20 kg was placed at (a, L, b). The structure was subjected to the

same acceleration as above ($n=1$) and the results by different models are shown in Table 5. The following comments arise from the analysis:

- Displacement results from classical, refined TE and LE models are in good agreement with the solid solution; even if classical EBBM theory is considered, the committed error ranges from

Table 4
u_z (m) at (a, L, b), σ_{yy} (MPa) at $(a/2, 0, b)$, and σ_{yz} (MPa) at $(a/2, L/2, 0)$. I-shaped beam undergoing a unitary load factor.

| Models	$-u_z \times 10^3$	σ_{yy}	$-\sigma_{yz} \times 10$	DOFs
	Classical models			
EBBM	0.306	1.530	0.000	93
TBM	0.310	1.530	0.395	155
	TE			
$N=2$	0.306	1.728	0.415	558
$N=4$	0.310	1.952	1.039	1395
$N=6$	0.311	2.108	1.145	2604
$N=7$	0.311	2.117	1.016	3348
	LE			
7 L9, Fig. 11	0.312	2.107	0.961	4185
	MSC Nastran			
Solid	0.314	1.923	1.020	127,800
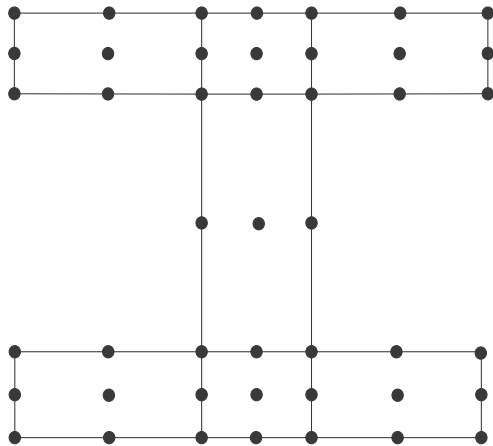
Fig. 11. Distribution of L9 elements above the cross-section of the I-shaped beam.

Table 5
u_z (m) at (a, L, b), σ_{yy} (MPa) at $(a/2, 0, b)$, and σ_{yz} (MPa) at $(a/2, L/2, 0)$. I-shaped beam undergoing a unitary load factor and a non-structural mass.

Models	$-u_z \times 10^3$	σ_{yy}	$-\sigma_{yz} \times 10$	DOFs
	Classical models			
EBBM	0.373	1.782	0.000	93
TBM	0.378	1.782	0.460	155
	TE			
$N=2$	0.375	2.013	0.483	558
$N=4$	0.382	2.250	1.210	1395
$N=6$	0.384	2.432	1.334	2604
$N=7$	0.385	2.441	1.181	3348
	LE			
7 L9, Fig. 11	0.388	2.430	1.045	4185
	MSC Nastran			
Solid	0.392	2.218	1.262	127,800

2.6% (uniform load factor without non-structural mass) to 4.8% (with structural mass) with respect to the solid FEM model. This is due to the fact that the analysed structure is more rigid in the cross-sectional plane if compared to the C-shaped beam of the previous section.

- Higher-order models are needed to correctly detect the stress state. In particular, as it is known, classical beam models are completely inadequate when shear stress components have to be computed.
- LE models detect the solid solution both in the case of symmetric and un-symmetric loading conditions. Displacement and stress results by the LE model agree in fact with those by the reference solution and a very few DOFs are used.
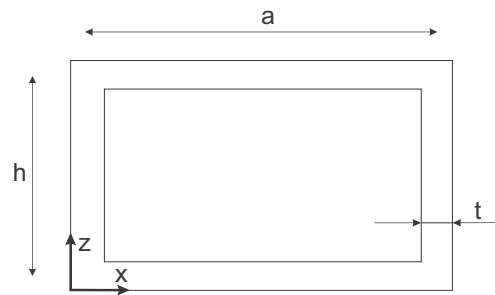
Fig. 12. Cross-section of the hollow-rectangular beam.

Table 6
Vertical displacement, u_z (mm), at $(a, L, 0)$. Hollow-rectangular beam undergoing a uniform gravitational load.

Models	$-u_z$	DOFs
	Classical models	
EBBM	0.589	93
TBM	0.593	155
	TE	
$N=2$	0.573	558
$N=4$	0.601	1395
$N=6$	0.619	2604
$N=7$	0.624	3348
$N=8$	0.624	4185
$N=9$	0.626	5115
	LE	
10 L9, Fig. 13a	0.626	5580
	MSC Nastran	
Solid	0.630	38,400

3.3. Closed and open hollow-rectangular beams

A cantilever closed hollow-rectangular cross-section was analysed. In Fig. 12 the cross-section of the beam is shown. The geometrical data are as follows: $a=0.8$ m, $h=0.2$ m and $t=0.01$ m. The length of the beam, L, was equal to 3.2 m. In the first analysis case, the structure underwent a uniform gravity acceleration load. A comparison between different models is proposed in Table 6. Classical as well as refined TE and LE beam models are compared to MSC Nastran© solid solution. The solid model was obtained by using the same brick elements as in the previous analysis cases. The LE model was obtained by using 10 L9 elements above the cross-section as shown in Fig. 13a. In Fig. 13a different notation with respect to Figs. 5 and 11 was used. In particular, the Lagrange points on the cross-section are not shown in Fig. 13 for the sake of clarity. A non-structural mass was applied next. The two following cases were addressed: in Case A the non-structural mass was placed at $(a, L, 0)$ as shown in Fig. 14a; in Case B (Fig. 14b) the mass was placed at $(a/2, L, h)$. The weight of the non-structural mass was equal to 10 kg. Table 7 collects the results from all the models implemented. Fig. 15 shows the tip cross-section deformation by LE models and MSC Nastran© solid model. Two different LE discretizations were addressed in this analysis case. Both a 10 L9 (Fig. 13a) and a 16 L9 (Fig. 13b) mesh were in fact considered. The following comments are noteworthy:

- Classical models are not able to foresee the mechanical behaviour of the hollow-rectangular beam.
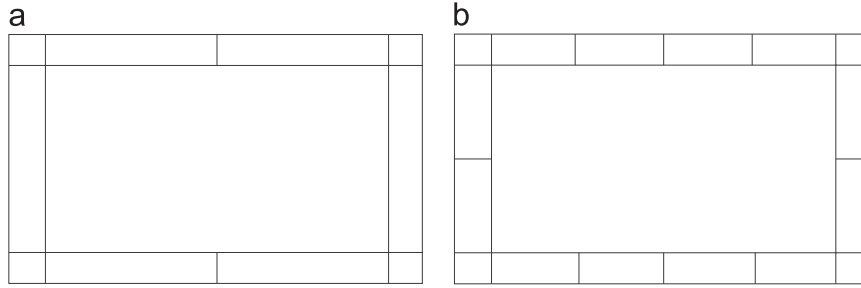- A TE model with at least a sixth-order expansion ($N=6$) is necessary if a uniform gravity load is considered.

Fig. 13. Distribution of L9 elements above the cross-section of the hollow-rectangular beam: (a) 10 L9 and (b) 16 L9.
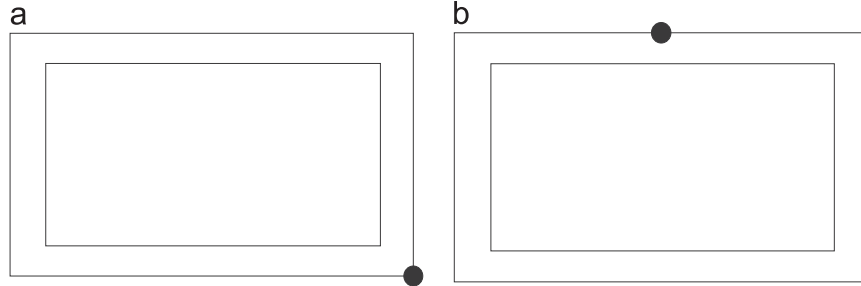

Fig. 14. Non-structural masses above the tip cross-section of the hollow-rectangular beam: (a) Case A and (b) Case B.

- Higher-order TE models can be effective when non-structural masses are placed so that torsional effects are predominant (Fig. 14a).
- If the non-structural mass is placed as in Fig. 14b, local phenomena occur and TE models are ineffective.
- Very good results are obtained by LE models both in the case of uniform and non-uniform loading conditions. However, if local effects occur, sufficiently enriched cross-sectional discretizations are needed to correctly detect the MSC Nastran$^{©}$ solid solution, as shown in Fig. 15.

A uniform angular acceleration was then applied to the structure. The magnitude of the acceleration was equal to -10^3 rad s^{-2} with respect to the y-axis. Table 8 quotes the cross-sectional displacement components measured at $(0, L, 0)$. It is clear that TE models are completely inefficient for the problem under consideration. This aspect is also confirmed by Fig. 16, in which the deformed configuration of the tip cross-section by both TE and LE models are compared to the MSC Nastran$^{©}$ solid solution.

An open hollow-rectangular beam as shown in Fig. 17 was addressed as the last example. The cross-sectional dimensions are the same as the closed hollow-rectangular beam discussed above. The only difference is that, in this case, a cut was made along the whole length of the beam. First, the structure underwent the following two point loads: one point load ($F_x = -500$ N) was applied at $(0, L, 0)$ and one load ($F_x = 500$ N) was applied at $(a, L, 0)$. Horizontal displacements were measured at $(a, L, 0)$ and the results are shown in Table 9.

The last analysis is focussed on the application of a non-uniform acceleration field to the open hollow-rectangular beam. Two non-structural masses equal to 10 kg were added as shown in Fig. 18 and the following acceleration was applied:

$$\ddot{u}_{x_0}(x, y, z) = \begin{cases} 1 g & \left(x > \dfrac{a}{2}\right) \\ -1 g & \left(x < \dfrac{a}{2}\right) \end{cases} \qquad (20)$$

The results are shown in Table 10, where LE models are compared to solid MSC Nastran$^{©}$ solution. Fig. 19 compares the deformed
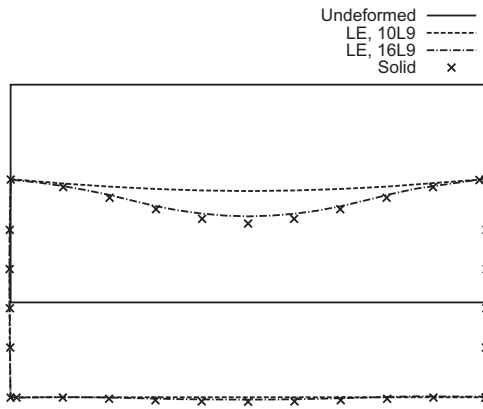
Table 7

Hollow-rectangular beam under uniform gravitational load. Effect due to the non-structural mass on the vertical displacement, u_z (mm), and on the shear stress, σ_{yz} (MPa).

Models	Case A, Fig. 14a		Case B, Fig. 14b		DOFs
	$-u_z$ @ $(a, L, 0)$	$-\sigma_{yz}$ @ $(a, L/2, h/2)$	$-u_z$ @ $(a/2, L, h)$	$-\sigma_{yz}$ @ $(a, L/2, h/2)$	
Classical models					
EBBM	0.680	0.000	0.680	0.000	93
TBM	0.686	0.047	0.686	0.047	155
TE					
$N=2$	0.665	0.087	0.662	0.081	558
$N=3$	0.694	0.313	0.691	0.307	930
$N=4$	0.697	0.323	0.694	0.308	1395
$N=5$	0.719	0.290	0.718	0.275	1953
$N=6$	0.720	0.288	0.724	0.275	2604
$N=7$	0.730	0.240	0.767	0.228	3348
$N=8$	0.731	0.237	0.817	0.227	4185
LE					
10 L9, Fig. 13a	0.748	0.251	0.813	0.243	5580
16 L9, Fig. 13b	0.759	0.268	1.006	0.254	8928
MSC Nastran					
Solid	0.761	0.259	1.062	0.254	38,400

configuration of the tip cross-section between the LE and solid model. From the analyses conducted it is clear that the present refined beam theories are able to deal with both uniform and non-uniform acceleration fields, since 3D-like phenomena can be detected. However, the following comments are worthy of investigations:

- LE models have to be preferred to TE models when rotational accelerations are accounted for or local phenomena occur.
- Classical and TE models are not suitable in the case of open cross-sections subjected to two opposite forces. Conversely, LE models are able to deal with cut cross-sections.

Fig. 15. Deformed tip cross-section of the hollow-rectangular beam undergoing inertial load and non-structural mass (Case B, Fig. 14b).

Table 8
Hollow-rectangular beam under uniform angular acceleration. Displacements components (mm) at $(0, L, 0)$.

| Models	u_x	u_z	DOFs
	TE		
$N=2$	0.124	-0.504	558
$N=3$	0.125	-0.521	930
$N=5$	0.123	-0.681	1953
$N=6$	0.126	-0.695	2604
	LE		
10 L9, Fig. 13a	-0.343	-2.453	5580
16 L9, Fig. 13b	-0.509	-3.120	8928
	MSC Nastran		
Solid	-0.533	-3.418	38,400
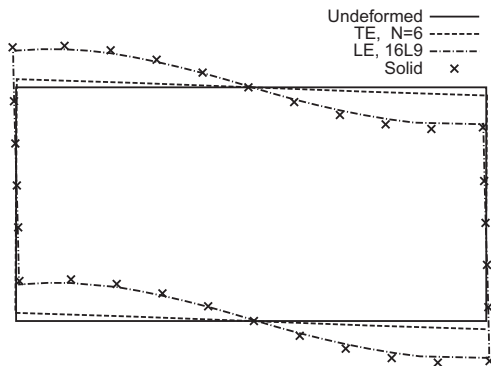
Fig. 16. Deformed tip cross-section of the hollow-rectangular beam undergoing uniform angular acceleration load.
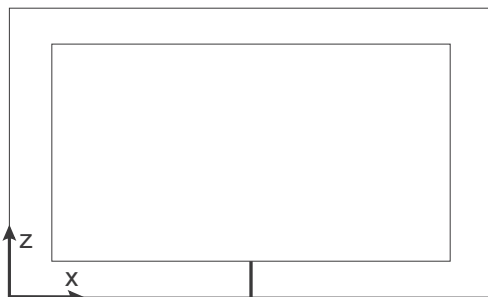
Fig. 17. Cross-section of the open hollow-rectangular beam.

Table 9
Horizontal displacement component, u_x (mm), at $(a, L, 0)$, open hollow-rectangular beam undergoing point loads.

Models	$-u_x$	DOFs
	Classical models	
EBBM	0	93
TBM	0	155
	TE	
$N=2$	0.002	558
$N=6$	0.004	2604
$N=8$	0.004	4185
$N=9$	0.005	5115
	LE	
10 L9, Fig. 13a	0.598	5580
16 L9, Fig. 13b	0.603	8928
	MSC Nastran	
Solid	0.611	38,400
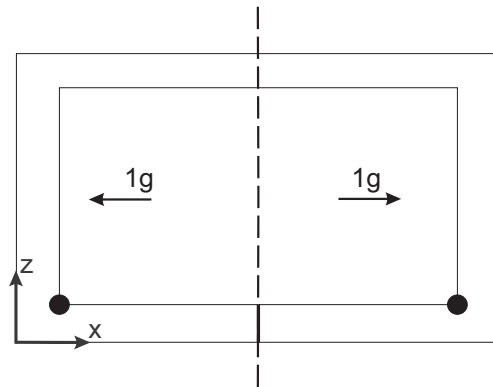
Fig. 18. Open hollow-rectangular beam with two non-structural masses undergoing a non-uniform acceleration field.

Table 10
Open hollow-rectangular beam undergoing non-uniform acceleration load. Displacement components (mm) at $(0, L, 0)$.

Models	$-u_x$	$-u_y$	$-u_z$	DOFs
	LE			
10 L9, Fig. 13a	0.261	0.020	0.232	5580
16 L9, Fig. 13b	0.273	0.021	0.242	8924
	MSC Nastran			
Solid	0.248	0.019	0.229	38,400

● Even tough acceleration fields that are non-constant above the cross-section are applied, LE models are able to replicate the MSC Nastran© solid results with very few degrees of freedom.

4. Conclusions

The effects of load factors and non-structural masses on the static response of beam structures have been investigated in the present paper. The analyses have been carried out by means of refined beam theories based on the Carrera Unified Formulation (CUF). CUF is a hierarchical formulation that allows higher-order displacement fields to be developed with no a priori kinematics assumptions. According to CUF, the displacement field is an expansion of generic functions above the cross-section. Different classes of refined beam models can be obtained, depending on the choice of the expanding functions. In this paper, both TE and LE refined models, which are based on Taylor-like and Lagrange polynomials, respectively, have been implemented.
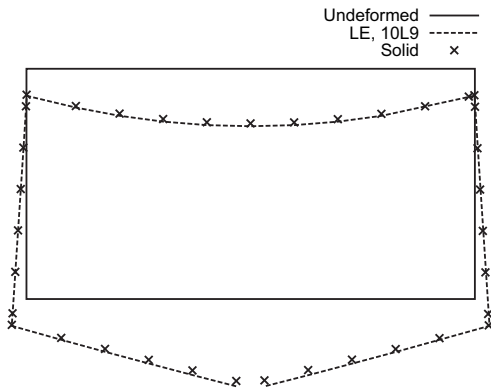
Fig. 19. Tip cross-section deformation of the hollow open beam subjected to non-uniform acceleration load and non-structural masses.

From the results that have been obtained, it is possible to draw the following conclusions:

- Classical beam theories are not suitable for the problems under consideration; classical theories are in fact not able to detect non-classical effects due to non-symmetric geometries or to load factors whose distribution above the cross-section is not con-stant. In general, arbitrary acceleration fields are considered as a combination of transversal and rotational load factors applied with reference to the shear axis, if classical beam theories are considered. Obviously, 3D effects cannot be detected.
- The adoption of refined models is therefore compulsory to detect local effects and the mechanical response of thin-walled beams subjected to rotational as well as non-uniform acceleration fields.
- Generally, higher-order TE models can be used if uniform load factors are applied and simple geometries are considered.
- As a general guideline, LE models are preferable to TE models, when bending/coupling effects play an important role, local deformations cannot be neglected, and an accurate description of the stress state is needed.

- From a comparison with the results obtained from solid element models, it is clear that LE theories provide good accuracy for all the assessed problems and the computational cost of the present beam formulation is considerably lower than those incurred for 3D solutions.

References

[1] Euler L. De curvis elasticis. Lausanne and Geneva: Bousquet; 1744 [W.A. Oldfather, C.A. Elvis, D.M. Brown, Leonhard Euler's elastic curves, Isis 1933;20:72–160].
[2] Timoshenko SP. On the corrections for shear of the differential equation for transverse vibrations of prismatic bars. Philos Mag 1922;41:744–6.
[3] Timoshenko SP. On the transverse vibrations of bars of uniform cross section. Philos Mag 1922;43:125–31.
[4] Novozhilov VV. Theory of elasticity. Elmsford: Pergamon; 1961.
[5] Kapania K, Raciti S. Recent advances in analysis of laminated beams and plates. Part I. shear effects and buckling. AIAA J 1989;27(7):923–35.
[6] Kapania K, Raciti S. Recent advances in analysis of laminated beams and plates. Part II. vibrations and wave propagation. AIAA J 1989;27(7):935–46.
[7] Timoshenko SP, Goodier JN. Theory of elasticity. New York, USA: McGraw-Hill;1970.
[8] Sokolnikoff IS. Mathematical theory of elasticity. New York, USA: McGraw-Hill; 1956.
[9] Stephen NG. Timoshenko's shear coefficient from a beam subjected to gravity loading. J Appl Mech 1980;47:121–7.
[10] Hutchinson JR. Shear coefficients for Timoshenko beam theory. J Appl Mech 2001;68:87–92.
[11] Nguyen TK, Vo TP, Thai HT. Static and free vibration of axially loaded functionally graded beams based on the first-order shear deformation theory. Compos Part B: Eng 2013;55:147–57.
[12] Kaneko T. On Timoshenko's correction for shear in vibrating beams. J Phys D: Appl Phys 1975;8:1927–36.
[13] Dong SB, Alpdongan C, Taciroglu E. Much ado about shear correction factors in Timoshenko beam theory. Int J Solids Struct 2010;47:1651–65.
[14] El Fatmi R. On the structural behavior and the Saint Venant solution in the exact beam theory: application to laminated composite beams. Comput Struct 2002;80(16–17):1441–56.
[15] El Fatmi R. A non-uniform warping theory for beams. Comptes Rendus – Mec 2007;335:467–74.
[16] Ladéveze P, Sanchez P, Simmonds JG. Beamlike (Saint-Venant) solutions for fully anisotropic elastic tubes of arbitrary closed cross-section. Int J Solids Struct 2004;41(7):1925–44.
[17] Ladéveze P, Simmonds JG. The exact one-dimensional theory for end-loaded fully anisotropie beams of narrow rectangular cross section. J Appl Mech 2001;68(6):865–8.
[18] Berdichevsky VL, Armanios E, Badir A. Theory of anisotropic thin-walled closed-cross-section beams. Compos Eng 1992;2(5–7):411–32.
[19] Rajagopal A, Hodges DH. Asymptotic approach to oblique cross-sectional analysis of beams. J Appl Mech 2014;81(3):031015.
[20] Wang Q, Yu W. A variational asymptotic approach for thermoelastic analysis of composite beams. Adv Aircr Spacecr Sci 2014;1(1):93–123.
[21] Yu W, Hodges DH. Elasticity solutions versus asymptotic sectional analysis of homogeneous, isotropic, prismatic beams. J Appl Mech 2004;71:15–23.
[22] Yu W, Hodges DH. Generalized Timoshenko theory of the variational asymptotic beam sectional analysis. J Am Helicopter Soc 2005;50(1):46–55.
[23] Kim JS, Wang KW. Vibration analysis of composite beams with end effects via the formal asymptotic method. J Vib Acoust 2010;132(4):041003.
[24] Schardt R. Verallgemeinerte technische biegetheorie. Berlin: Springer; 1989.
[25] Schardt R. Generalized beam theory an adequate method for coupled stability problems. Thin-Walled Struct 1994;19:161–80.
[26] Silvestre N. Generalised beam theory to analyse the buckling behaviour of circular cylindrical shells and tubes. Thin-Walled Struct 2007;45(2):185–98.
[27] Nunes F, Correia M, Correia JR, Silvestre N, Moreira A. Experimental and numerical study on the structural behavior of eccentrically loaded GFRP columns. Thin-Walled Struct 2013;72:175–87.
[28] Silvestre N, Camotim D. Shear deformable generalized beam theory for the analysis of thin-walled composite members. J Eng Mech 2013;139(8):1010–24.
[29] De Miranda S, Gutierrez A, Miletta R. Equilibrium-based reconstruction of three-dimensional stresses in GBT. Thin-Walled Struct 2014;74:146–54.
[30] Carrera E. A class of two-dimensional theories for multilayered plates analysis. Atti Accad delle Sci di Torino, Mem Sci Fis 1995;19–20:49–87.
[31] Carrera E. Theories and finite elements for multilayered, anisotropic, composite plates and shells. Arch Comput Methods Eng 2002;9(2):87–140.
[32] Carrera E. Theories and finite elements for multilayered plates and shells: a unified compact formulation with numerical assessment and benchmarking. Arch Comput Methods Eng 2003;10(3):216–96.
[33] Carrera E, Giunta G. Refined beam theories based on a unified formulation. Int J Appl Mech 2010;2(1):117–43, http://dx.doi.org/10.1142/S1758825110000500.
[34] Carrera E, Giunta G, Petrolo M. Beam structures: classical and advanced theories. Chichester, UK: John Wiley & Sons; http://dx.doi.org/10.1002/9781119978565.
[35] Carrera E, Giunta G, Nali P, Petrolo M. Refined beam elements with arbitrary cross-section geometries. Comput Struct 2010;88(5-6):283–93, http://dx.doi.org/10.1016/j.compstruc.2009.11.002.
[36] Carrera E, Petrolo M, Zappino E. Performance of CUF approach to analyze the structural behavior of slender bodies. J Struct Eng 2012;138(2):285–97, http: //dx.doi.org/10.1061/(ASCE)ST.1943-541X.0000402.
[37] Carrera E, Petrolo M, Nali P. Unified formulation applied to free vibrations finite element analysis of beams with arbitrary section. Shock Vib 2011;18 (3):485–502, http://dx.doi.org/10.3233/SAV-2010-0528.
[38] Pagani A, Boscolo M, Banerjee JR, Carrera E. Exact dynamic stiffness elements based on one-dimensional higher-order theories for free vibration analysis of solid and thin-walled structures. J Sound Vib 2013;332(23):6104–27, http: //dx.doi.org/10.1016/j.jsv.2013.06.023.
[39] Petrolo M, Zappino E, Carrera E. Refined free vibration analysis of one-dimensional structures with compact and bridge-like cross-sections. Thin-Walled Struct 2012;56:49–61, http://dx.doi.org/10.1016/j.tws.2012.03.011.
[40] Carrera E, Petrolo M. Refined beam elements with only displacement variables and plate/shell capabilities. Meccanica 2012;47(3):537–56, http://dx.doi.org/10.1007/s11012-011-9466-5.
[41] Carrera E, Petrolo M. Refined one-dimensional formulations for laminated structure analysis. AIAA J 2012;50(1):176–89, http://dx.doi.org/10.2514/1.J051219.
[42] Carrera E, Pagani A, Petrolo M. Classical refined and component-wise theories for static analysis of reinforced-shell wing structures. AIAA J 2013;51 (5):1255–68, http://dx.doi.org/10.2514/1.J052331.
[43] Carrera E, Zappino E, Petrolo M. Analysis of thin-walled structures with longitudinal and transversal stiffeners. J Appl Mech 2013;80:011006, http: //dx.doi.org/10.1115/1.4006939.
[44] Carrera E, Pagani A, Petrolo M. Refined 1d finite elements for the analysis of secondary, primary and complete civil engineering structures; 2014 (submitted for publication).
[45] Carrera E, Pagani A. Free vibration analysis of civil engineering structures by component-wise models; 2014 (submitted for publication).
[46] Bathe KJ. Finite element procedure. Upper Saddle River, New Jersey, USA: Prentice Hall; 1996.